Reduced-order Aggregate Model for Parallel-connected Grid-tied Three-phase Photovoltaic Inverters

Victor Purba[†], Brian B. Johnson[§], and Sairaj V. Dhople[†]

[†]University of Minnesota, Minneapolis, MN, 55455, [§]University of Washington, Seattle, WA, 98195

***Abstract*—Ratings of utility-scale grid-tied photovoltaic (PV) inverters are typically no more than $1\,\mathrm{MVA}$. This implies that a large number of inverters are usually installed in utility-scale PV energy-conversion systems. Given the complexity of inverter dynamic models (typical models are high dimension and nonlinear), reduced-order models for inverters are critical for performance assessment and accurate representation of PV-system dynamics in the bulk power grid with limited computational burden. In this paper, we formulate a reduced-order model for parallel-connected grid-tied three-phase PV inverters that has the same structure and model order as a single inverter. We adopt a single-diode model for the PV modules, and each inverter is assumed to be a single-stage dc-ac voltage-source converter with an input dc-link capacitor and an LCL output filter. The control architecture includes a maximum power point tracking (MPPT) algorithm, a dc-link voltage controller, a reactive power controller, a current controller, and a phase-locked loop for grid synchronization. Numerical simulations demonstrate the computational benefits and accuracy of the reduced-order model.**

***Index Terms*—Maximum power point tracking, model reduction, photovoltaic inverter, three-phase inverter.**

I. Introduction

In 2017, 31% of all U.S. capacity additions (corresponding to $6.2\,\mathrm{GW}$) were in the form of utility-scale photovoltaic (PV) systems, and these accounted for 60% of newly installed solar capacity [1]. Power-electronics inverters interface PV arrays to the grid, and given typical ratings of constituent power-semiconductor devices and filters, PV plants with as many as thousands of inverters are not uncommon [2]. As PV plants will serve a significant portion of loads in the future power system, it is critical to develop scalable and accurate models that capture the collective dynamics of inverters to facilitate integration in bulk-system models.

With a view towards facilitating computationally inexpensive modeling of utility-scale PV plants, this paper proposes an aggregate reduced-order model for grid-tied three-phase PV inverters. We focus on the voltage-source inverter (VSI) model illustrated in Fig. 1. It is composed of a PV array, a dc-link capacitor, output LCL filter, and the control architecture includes a pulse width modulation (PWM) scheme, current controller, a perturb & observe (P&O) maximum power point tracking (MPPT) algorithm, dc-link voltage and reactive power controllers, and a phase-locked loop (PLL) for grid synchronization. This PV-inverter model (and closely related variants) are fairly common in the literature [3]–[6]. The corresponding state-space dynamic model for such an inverter is nonlinear and has more than 10 dynamical states, which implies that studying large collections of such inverters in a PV system with all states explicitly modeled is not practical. To address this issue, we derive a reduced-order model for parallel-connected PV inverters that has the same structure and order as the individual inverter. In other words, the reduced-order model is also composed of (an equivalent) PV array, dc-link capacitor, LCL filter, current controller, MPPT algorithm, PLL, and dc-link-voltage and reactive-power controllers. We provide pertinent scalings for controller and filter parameters from the original inverter model so that the corresponding reduced-order model precisely captures the input-output behavior of the original system of paralleled inverters. Our aggregation results focus on the following two cases: the first case is when the PV arrays are uniformly illuminated and all model and control parameters are homogeneous, and the second case is when the PV arrays are exposed to different values of solar irradiance and the frequency and perturbation size for the P&O MPPT algorithms are not all the same.

Related prior work in this domain is predominantly focused on reduced-order models for individual inverters [7]–[9]. Recent work on reduced-order models for collections of grid-tied inverters include [10]–[13], and models incorporating network impacts include [14]–[16]. The reduced-order model proposed in this work extends [10] to acknowledge the PV array, MPPT algorithm, and dc-link capacitor dynamics. This work also differs from the aggregated models for PV inverters studied in [12], since it provides a systematic way of scaling the PV and control parameters based on the number of inverters. The reduced-order model has similar model complexity as a synchronous machine model, and thus facilitates the accurate representation of PV plants in bulk transmission-scale models with limited computational burden. In this regard, we anticipate applications for the reduced-order model in power quality studies [17], stability analysis for systems with high PV penetration [18]–[20], and evaluating opportunities for frequency support by PV systems [21]. Finally, with minor extensions, the general aggregation strategy outlined here can also be extended to grid-forming controllers, see, e.g., [22].

The remainder of this paper is organized as follows. In Section II, we introduce the grid-tied three-phase PV inverter model. In Section III, we derive the reduced-order model for parallel-connected PV inverters in the homogeneous setting, and describe extensions to the model for different solar irradiance and parameters of the MPPT algorithms. In Section IV, we provide comparative numerical simulations of a parallel-connected system and its corresponding reduced-

978-1-7281-0494-2/19/$31.00 ©2019 IEEE

order model. Concluding remarks and directions for future work are provided in Section V.

II. Model Description

A block diagram illustrating the PV array, feedback controllers, and output filters in the grid-tied three-phase voltage-source inverter (VSI) is given in Fig. 1. The controllers consist of a phase-locked loop, a maximum power point algorithm, a dc-link & power controller, and a current controller. The PV inverter is assumed to operate at unity power factor. We briefly overview important attributes of this model next.

A. Model of PV Array

Each inverter is connected to an array composed of N_p strings of N_s series-connected modules. We adopt a single-diode model with a parallel output resistance, R_p, for each module [23], [24]. The output current of the PV array is:

$$i_\mathrm{pv} = N_\mathrm{p}\left(i_\mathrm{ph} - i_\mathrm{rs}\left(\mathrm{e}^{\frac{q\,v_\mathrm{dc}}{N_\mathrm{m}KTN_\mathrm{s}}} - 1\right) - \frac{v_\mathrm{dc}}{N_\mathrm{s}R_\mathrm{p}}\right), \quad (1)$$

where i_ph is the photocurrent that depends on the solar irradiance, i_rs is the reverse saturation current, q is the electron charge, v_dc is the voltage across the dc-link capacitor, N_m is the number of cells in a module, K is the Boltzmann constant, and T is the surface temperature of the module.

B. Dc- and ac-side Filters

The inverter is composed of two filters, a dc-side capacitive filter and an ac-side LCL filter. The LCL filter (L_i, C_f, L_g) connects the switched terminal of the voltage-sourced inverter (VSI) to the grid. The states of the filter are the inverter terminal currents i_i^d and i_i^q, where superscripts d and q denote the d- and q- components of the current, the filter voltages v_f^d and v_f^q, and output currents i_o^d and i_o^q (transforming the balanced three phase signals to the dq-reference frame is done using Park's Transformation; see [10], [25] for details). Denote $i_\mathrm{i}^\mathrm{dq} := [i_\mathrm{i}^\mathrm{d}, i_\mathrm{i}^\mathrm{q}]^\mathrm{T}$, $i_\mathrm{o}^\mathrm{dq} := [i_\mathrm{o}^\mathrm{d}, i_\mathrm{o}^\mathrm{q}]^\mathrm{T}$, $v_\mathrm{i}^\mathrm{dq} := [v_\mathrm{i}^\mathrm{d}, v_\mathrm{i}^\mathrm{q}]^\mathrm{T}$, $v_\mathrm{f}^\mathrm{dq} := [v_\mathrm{f}^\mathrm{d}, v_\mathrm{f}^\mathrm{q}]^\mathrm{T}$, and $v_\mathrm{g}^\mathrm{dq} := [v_\mathrm{g}^\mathrm{d}, v_\mathrm{g}^\mathrm{q}]^\mathrm{T}$. The dynamics of the states corresponding to the LCL filter in the dq domain are:

$$\dot{i}_\mathrm{i}^\mathrm{dq} = \frac{1}{L_\mathrm{i}}(-R_\mathrm{i} i_\mathrm{i}^\mathrm{dq} + v_\mathrm{i}^\mathrm{dq} - v_\mathrm{f}^\mathrm{dq}) + \Gamma\omega_\mathrm{PLL} i_\mathrm{i}^\mathrm{dq}, \quad (2)$$

$$\dot{i}_\mathrm{o}^\mathrm{dq} = \frac{1}{L_\mathrm{g}}(-R_\mathrm{g} i_\mathrm{o}^\mathrm{dq} + v_\mathrm{f}^\mathrm{dq} - v_\mathrm{g}^\mathrm{dq}) + \Gamma\omega_\mathrm{PLL} i_\mathrm{o}^\mathrm{dq}, \quad (3)$$

$$\dot{v}_\mathrm{f}^\mathrm{dq} = R_\mathrm{f}(\dot{i}_\mathrm{i}^\mathrm{dq} - \dot{i}_\mathrm{o}^\mathrm{dq}) - \Gamma\omega_\mathrm{PLL} R_\mathrm{f}(i_\mathrm{i}^\mathrm{dq} - i_\mathrm{o}^\mathrm{dq}) + \frac{1}{C_\mathrm{f}}(i_\mathrm{i}^\mathrm{d} - i_\mathrm{o}^\mathrm{dq}) + \Gamma\omega_\mathrm{PLL} v_\mathrm{f}^\mathrm{dq}, \quad (4)$$

where $\Gamma = \begin{bmatrix} 0 & 1 \\ -1 & 0 \end{bmatrix}$, and ω_PLL denotes the PLL frequency.

The dc-link capacitor, C_dc, interfaces the PV array to the inverter. It is designed to minimize the current ripple imposed on the PV array. The state of the filter is the energy stored in the capacitor, $e_\mathrm{dc} := v_\mathrm{dc}^2$. Assuming lossless operation of the switches in the VSI, the dynamics of e_dc are:

$$\dot{e}_\mathrm{dc} = \frac{1}{C_\mathrm{dc}}(p_\mathrm{pv} - p_\mathrm{i}), \quad (5)$$

where p_pv and p_i denote the power sourced by the PV array and the real power calculated at the terminals of the inverter:

$$p_\mathrm{pv} = v_\mathrm{dc} i_\mathrm{pv}, \quad p_\mathrm{i} = \frac{3}{2}(v_\mathrm{i}^\mathrm{d} i_\mathrm{i}^\mathrm{d} + v_\mathrm{i}^\mathrm{q} i_\mathrm{i}^\mathrm{q}). \quad (6)$$

C. Phase-locked Loop (PLL)

The PLL consists of a PI controller (with PI gains k_PLL^p and k_PLL^i) and a low pass filter (with cut-off frequency of $\omega_\mathrm{c,PLL}$). The output of the PI controller is the PLL frequency:

$$\dot{\delta} =: \omega_\mathrm{PLL} = 2\pi \times 60 - k_\mathrm{PLL}^p v_\mathrm{PLL} - k_\mathrm{PLL}^i \int v_\mathrm{PLL} dt, \quad (7)$$

where v_PLL denotes the output of the low pass filter with the following dynamics:

$$\dot{v}_\mathrm{PLL} = \omega_\mathrm{c,PLL}(v_\mathrm{g}^\mathrm{d} - v_\mathrm{PLL}). \quad (8)$$

The PLL dynamics ensure that $v_\mathrm{g}^\mathrm{d} \to 0$, which amounts to tracking the phase-a grid-side voltage. To simplify notation in subsequent developments, we define the following: $\dot{\phi}_\mathrm{PLL} = -v_\mathrm{PLL}$.

D. Maximum Power Point Tracking (MPPT) Algorithm

We assume that the perturb and observe (P&O) algorithm is utilized to track the maximum power point (MPP). The basic premise of this algorithm is to perturb the dc-link voltage reference in a direction to increase the power drawn from the PV array. To facilitate computations with accuracy, a low-pass filter with cut-off frequency, $\omega_\mathrm{c,pv}$, yields an averaged PV output power, $p_\mathrm{pv,avg}$, that is utilized in the algorithm:

$$\dot{p}_\mathrm{pv,avg} = \omega_\mathrm{c,pv}(p_\mathrm{pv} - p_\mathrm{pv,avg}). \quad (9)$$

The update for the dc-link voltage reference is given by: [26]

$$v_\mathrm{dc}^\star(t+\tau) = v_\mathrm{dc}^\star(t) + \rho \cdot \mathrm{sgn}(\Delta v_\mathrm{dc}(t))\mathrm{sgn}(\Delta p_\mathrm{pv,avg}(t)), \quad (10)$$

where ρ denotes the perturbation size, τ denotes the perturbation period, $\mathrm{sgn}(\cdot)$ denotes the signum function, and

$$\Delta v_\mathrm{dc}(t) = v_\mathrm{dc}(t) - v_\mathrm{dc}(t-\tau), \quad (11)$$

$$\Delta p_\mathrm{pv,avg}(t) = p_\mathrm{pv,avg}(t) - p_\mathrm{pv,avg}(t-\tau), \quad (12)$$

denote the change in dc-link voltage and corresponding change in averaged PV output power, respectively.

E. Dc-link & Power Controller

The controller consists of a dc-link voltage controller and a reactive power controller. The dc-link voltage controller is composed of a PI controller (with PI gains k_VC^p and k_VC^i). The reference to the controller is the dc-link energy setpoint, $e_\mathrm{dc}^\star$, which is equal to the square of dc-link voltage setpoint, $v_\mathrm{dc}^\star$, i.e., $e_\mathrm{dc}^\star = v_\mathrm{dc}^{\star 2}$. The output is the reference for i_i^q:

$$i_\mathrm{i}^{\mathrm{q}\star} = -k_\mathrm{VC}^p(e_\mathrm{dc}^\star - e_\mathrm{dc}) - k_\mathrm{VC}^i \int (e_\mathrm{dc}^\star - e_\mathrm{dc})\, dt. \quad (13)$$

The reactive power controller is composed of a PI controller (with PI gains k_Q^p and k_Q^i) and a low-pass filter (with cut-off frequency $\omega_\mathrm{c,Q}$). If the inverter operates at unity power

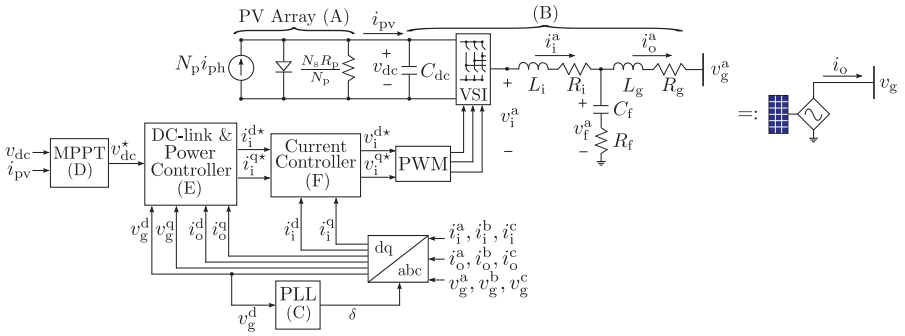

Fig. 1. Block diagram of the grid-tied three-phase PV inverter (left) and shorthand representation adopted for the same (right). The PV array is represented with a single-diode model. A single leg of the LCL filter corresponding to the a phase is depicted. Variables super-scripted by $\mathrm{a}, \mathrm{b}, \mathrm{c}$ denote the time-domain ac waveforms for the respective phases, while those super-scripted by d, q correspond to those in the dq reference frame computed with the PLL angle, δ serving as the transformation angle. The inverter subsystems are marked with the corresponding subsection labels in Section II to facilitate exposition.

factor, the reactive power reference is zero. The output is the reference for $i_{\mathrm{i}}^{\mathrm{d}}$:

$$i_{\mathrm{i}}^{\mathrm{d}\star} = -k_{\mathrm{Q}}^{p} q_{\mathrm{avg}} - k_{\mathrm{Q}}^{i} \int q_{\mathrm{avg}}\, dt, \tag{14}$$

where q_{avg} is the output of the low pass filter:

$$\dot{q}_{\mathrm{avg}} = \omega_{\mathrm{c,Q}}(q - q_{\mathrm{avg}}), \tag{15}$$

where q is the instantaneous reactive power at the output:

$$q = \frac{3}{2}(v_{\mathrm{g}}^{\mathrm{q}} i_{\mathrm{o}}^{\mathrm{d}} - v_{\mathrm{g}}^{\mathrm{d}} i_{\mathrm{o}}^{\mathrm{q}}). \tag{16}$$

We define the following variables to simplify notation subsequently: $\dot{\phi}_{\mathrm{dc}} = e_{\mathrm{dc}}^{\star} - e_{\mathrm{dc}}$, $\dot{\phi}_{\mathrm{q}} = -q_{\mathrm{avg}}$.

F. Current Controller

The current controller consists of two PI controllers (with PI gains k_{CC}^{p} and k_{CC}^{i}), with output to be the reference for the inverter terminal voltage, $v_{\mathrm{i}}^{\mathrm{d}\star}$ and $v_{\mathrm{i}}^{\mathrm{q}\star}$:

$$\begin{aligned} v_{\mathrm{i}}^{\mathrm{d}\star} &= k_{\mathrm{CC}}^{p}(i_{\mathrm{i}}^{\mathrm{d}\star} - i_{\mathrm{i}}^{\mathrm{d}}) + k_{\mathrm{CC}}^{i} \int (i_{\mathrm{i}}^{\mathrm{d}\star} - i_{\mathrm{i}}^{\mathrm{d}})\, dt - \omega_{\mathrm{PLL}} L_{\mathrm{f}} i_{\mathrm{i}}^{\mathrm{q}}, \\ v_{\mathrm{i}}^{\mathrm{q}\star} &= k_{\mathrm{CC}}^{p}(i_{\mathrm{i}}^{\mathrm{q}\star} - i_{\mathrm{i}}^{\mathrm{d}}) + k_{\mathrm{CC}}^{i} \int (i_{\mathrm{i}}^{\mathrm{d}\star} - i_{\mathrm{i}}^{\mathrm{d}})\, dt + \omega_{\mathrm{PLL}} L_{\mathrm{f}} i_{\mathrm{i}}^{\mathrm{d}}. \end{aligned} \tag{17}$$

These voltage references are assumed to be instantaneously realized at the switched terminals of the VSI. To facilitate discussion, we define: $\dot{\gamma}^{\mathrm{d}} = i_{\mathrm{i}}^{\mathrm{d}\star} - i_{\mathrm{i}}^{\mathrm{d}}$, $\dot{\gamma}^{\mathrm{q}} = i_{\mathrm{i}}^{\mathrm{q}\star} - i_{\mathrm{i}}^{\mathrm{q}}$.

G. State-space Representation

The dynamics of the inverter can be represented in a compact state-space form as follows: $\dot{x} = Ax + g(x, u_1, u_2, u_3)$, where the states and inputs are:

$$\begin{aligned} x = [&i_{\mathrm{i}}^{\mathrm{d}}, i_{\mathrm{i}}^{\mathrm{q}}, i_{\mathrm{o}}^{\mathrm{d}}, i_{\mathrm{o}}^{\mathrm{q}}, v_{\mathrm{f}}^{\mathrm{d}}, v_{\mathrm{f}}^{\mathrm{q}}, e_{\mathrm{dc}}, p_{\mathrm{pv,avg}}, \phi_{\mathrm{dc}}, \\ &q_{\mathrm{avg}}, \phi_{\mathrm{q}}, \gamma^{\mathrm{d}}, \gamma^{\mathrm{q}}, v_{\mathrm{PLL}}, \phi_{\mathrm{PLL}}, \delta]^{\mathrm{T}}, \end{aligned} \tag{18}$$

$$u_1 = v_{\mathrm{dc}}^{\star}, \quad u_2 = [v_{\mathrm{g}}^{\mathrm{a}}, v_{\mathrm{g}}^{\mathrm{b}}, v_{\mathrm{g}}^{\mathrm{c}}]^{\mathrm{T}}, \quad u_3 = i_{\mathrm{ph}}. \tag{19}$$

Note that the dc-link voltage setpoint, $v_{\mathrm{dc}}^{\star}$, is obtained from the MPPT algorithm. Entries of $A \in \mathbb{R}^{16\times 16}$ and $g : \mathbb{R}^{16} \times \mathbb{R}^3 \times \mathbb{R} \to \mathbb{R}^{16}$ are in the Appendix.

III. Reduced-order Aggregated Model

We now derive a reduced-order aggregate model for a collection of N identical inverters with the same PV array configuration, connected in parallel. Following this homogeneous setup, we briefly overview some practicalities for heterogeneous settings.

A. Aggregation in Homogeneous Settings

In order to derive the aggregate reduced-order model, we scale the following parameters corresponding to the inverter controllers and PV array:

$$\begin{aligned} &\big(i_{\mathrm{rs}}, R_{\mathrm{p}}, C_{\mathrm{dc}}, L_{\mathrm{i}}, C_{\mathrm{f}}, L_{\mathrm{g}}, k_{\mathrm{VC}}^{p}, k_{\mathrm{VC}}^{i}, k_{\mathrm{CC}}^{p}, k_{\mathrm{CC}}^{i}\big) \to (N i_{\mathrm{rs}}, \\ &\quad \frac{R_{\mathrm{p}}}{N}, N C_{\mathrm{dc}}, \frac{L_{\mathrm{i}}}{N}, N C_{\mathrm{f}}, \frac{L_{\mathrm{g}}}{N}, N k_{\mathrm{VC}}^{p}, N k_{\mathrm{VC}}^{i}, \frac{k_{\mathrm{CC}}^{p}}{N}, \frac{k_{\mathrm{CC}}^{i}}{N}\Big). \end{aligned}$$

Parameters not mentioned above are unchanged. In particular, note that the PLL and reactive power controller parameters, and the frequency of any low pass filter are unchanged. With these scaled parameters, the resulting aggregate reduced-order model is illustrated in Fig. 2. We draw attention to the fact that this model has the same model order and structure as any individual PV inverter model in the parallel setup. Certain aspects of this model derive straightforwardly from elementary circuit theory. This is particularly obvious for the PV array and the output LCL filter. Given the parallel setup, we can see that the impedance corresponding to the LCL output filter in the reduced-order aggregate model is $1/N$ of that in the individual inverter. Similarly, the equivalent PV array for the aggregation is obtained from a parallel connection of N single-diode models for the individual arrays.

Formally, the dynamical model of the reduced-order equivalent has the following state-space form: $\dot{x}^{\mathrm{r}} = A^{\mathrm{r}} x^{\mathrm{r}} + g^{\mathrm{r}}(x^{\mathrm{r}}, u_1^{\mathrm{r}}, u_2^{\mathrm{r}}, u_3^{\mathrm{r}})$, where the states and the inputs are:

$$\begin{aligned} x^{\mathrm{r}} = [&i_{\mathrm{i}}^{\mathrm{d,r}}, i_{\mathrm{i}}^{\mathrm{q,r}}, i_{\mathrm{o}}^{\mathrm{d,r}}, i_{\mathrm{o}}^{\mathrm{q,r}}, v_{\mathrm{f}}^{\mathrm{d,r}}, v_{\mathrm{f}}^{\mathrm{q,r}}, e_{\mathrm{dc}}^{\mathrm{r}}, p_{\mathrm{pv,avg}}^{\mathrm{r}}, \phi_{\mathrm{dc}}^{\mathrm{r}}, \\ &q_{\mathrm{avg}}^{\mathrm{r}}, \phi_{\mathrm{q}}^{\mathrm{r}}, \gamma^{\mathrm{d,r}}, \gamma^{\mathrm{q,r}}, v_{\mathrm{PLL}}^{\mathrm{r}}, \phi_{\mathrm{PLL}}^{\mathrm{r}}, \delta^{\mathrm{r}}]^{\mathrm{T}}, \end{aligned} \tag{20}$$

$$u_1^{\mathrm{r}} = v_{\mathrm{dc}}^{\star,\mathrm{r}}, \quad u_2^{\mathrm{r}} = [v_{\mathrm{g}}^{\mathrm{a}}, v_{\mathrm{g}}^{\mathrm{b}}, v_{\mathrm{g}}^{\mathrm{c}}]^{\mathrm{T}}, \quad u_3^{\mathrm{r}} = N i_{\mathrm{ph}}. \tag{21}$$

All signals above with superscript r correspond contextually to their counterparts for the individual inverter model as

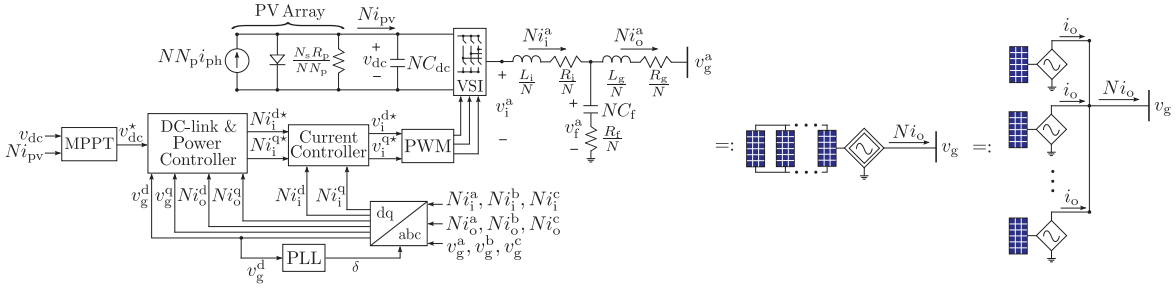

Fig. 2. Reduced-order aggregated PV inverter model for N parallel-connected inverters (left) and its adopted shorthand (center). This model precisely captures the output current and power injected by the parallel combination of N PV inverters (right). Scaling of parameters corresponding to equivalent PV array and LCL filter acknowledge the parallel interconnection of pertinent circuit elements.

discussed in Section II. For instance, $v_{\rm dc}^{\star,{\rm r}}$ denotes the dc-link voltage reference for the reduced-order model, generated from the corresponding MPPT algorithm. Inputs also have the same connotation, except notice that $u_3^{\rm r}$ captures N times the photocurrent, $i_{\rm ph}$. The matrix $A^{\rm r} \in \mathbb{R}^{16\times 16}$ and function $g^{\rm r} : \mathbb{R}^{16} \times \mathbb{R}^3 \times \mathbb{R} \to \mathbb{R}^{16}$ have the same structure and dimension as A and g.

We now establish the main result of this paper, whereby the current- and power-related states of the reduced-order aggregate model are noted to be N times those in the individual inverter model, while the voltage- and PLL-related states are the same.

Lemma 1. Consider the state-space model for the individual PV inverter. Permute x in (18) as

$$\widehat{x} = [i_{\rm i}^{\rm d}, i_{\rm i}^{\rm q}, i_{\rm o}^{\rm d}, i_{\rm o}^{\rm q}, p_{\rm pv,avg}, q_{\rm avg}, \phi_{\rm q}, \gamma^{\rm d}, \gamma^{\rm q}, v_{\rm f}^{\rm d}, v_{\rm f}^{\rm q}, e_{\rm dc}, \phi_{\rm dc}, v_{\rm PLL}, \phi_{\rm PLL}, \delta]^{\rm T}, \tag{22}$$

and also permute $x^{\rm r}$ in (20) the same way, denoting the permuted vector by $\widehat{x}^{\rm r}$. Suppose the initial conditions at time t_0 are such that $\widehat{x}^{\rm r}(t_0) = {\rm diag}(\psi)\widehat{x}(t_0)$, where $\psi := [\mathbb{1}_9^{\rm T}, \mathbb{1}_7^{\rm T}]^{\rm T}$, and the inputs are $u_1^{\rm r} = u_1, u_2^{\rm r} = u_2, u_3^{\rm r} = Nu_3$. It follows that $\forall t \geq t_0$, $\widehat{x}^{\rm r}(t) = {\rm diag}(\psi)\widehat{x}(t)$. In other words, the states of the reduced-order model and the individual inverter model are related as follows $\forall t \geq t_0$:

$$[i_{\rm i}^{\rm d,r}, i_{\rm i}^{\rm q,r}, i_{\rm o}^{\rm d,r}, i_{\rm o}^{\rm q,r}, p_{\rm pv,avg}^{\rm r}, q_{\rm avg}^{\rm r}, \phi_{\rm q}^{\rm r}, \gamma^{\rm d,r}, \gamma^{\rm q,r}]^{\rm T} = N[i_{\rm i}^{\rm d}, i_{\rm i}^{\rm q}, i_{\rm o}^{\rm d}, i_{\rm o}^{\rm q}, p_{\rm pv,avg}, q_{\rm avg}, \phi_{\rm q}, \gamma^{\rm d}, \gamma^{\rm q}], \tag{23}$$

$$[v_{\rm f}^{\rm d,r}, v_{\rm f}^{\rm q,r}, e_{\rm dc}^{\rm r}, \phi_{\rm dc}^{\rm r}, v_{\rm PLL}^{\rm r}, \phi_{\rm PLL}^{\rm r}, \delta^{\rm r}]^{\rm T} = [v_{\rm f}^{\rm d}, v_{\rm f}^{\rm q}, e_{\rm dc}, \phi_{\rm dc}, v_{\rm PLL}, \phi_{\rm PLL}, \delta]. \tag{24}$$

Proof. This can be proved in the same manner as in [10]. □

B. Aggregation in Heterogeneous Settings

We look into the following heterogeneous settings: #1) Inverters have different perturbation size and frequency for the P&O MPPT algorithm. #2) Inverters are exposed to different values of incident irradiance. For case #1, the dc-link voltage reference for the reduced-order model is updated in the same manner as (10), except, with perturbation size, ρ, and period, τ, selected to be the average of the perturbation size and period for the individual PV inverters. For case #2, the irradiance for the reduced-order model is the sum of the irradiance values of the individual inverters. While we are only able to analytically establish dynamic scaling of pertinent states in the homogeneous setting (see Lemma 1), the approach suggested above to contend with heterogeneity is empirically established through simulations to yield acceptable performance.

IV. Simulation Results

We compare results from simulating all the dynamics of a system of $N = 10$ parallel-connected PV inverters and the corresponding reduced-order aggregated model. Parameters are adopted from the Schneider Electric Conext CL125 string inverter [27] (power rating $125\,{\rm kW}$ and voltage rating $600\,{\rm V(rms)}$) and the First Solar FS-6420 [28] PV module (power rating $420\,{\rm W}$ and open-circuit voltage $218.5\,{\rm V}$). The PV array interfaced to each inverter consists of $N_{\rm p} = 60$ strings, with each string comprising $N_{\rm s} = 5$ series-connected PV modules. Filter and controller parameters are in Table I. These parameters are a scaled version of those in [11].

The solar irradiance data for this simulation is sourced from NREL's Oahu Solar Measurement Grid on July 24, 2011, for the time period 09:30:00 to 09:30:10 AM [29]. The data is then interpolated from 1- to 0.1-second step intervals (see Fig. 3a). We consider the following cases: #1) For all inverters, the period and perturbation size of the MPPT algorithm are selected to be uniformly distributed between $5-10\,{\rm ms}$ and $50-70\,{\rm mV}$, respectively. #2) Same setup as #1, but the solar irradiance corresponding to each inverter varies between $\pm 20\%$ of the nominal value as shown in Fig. 4a (for three selected inverters). The simulations were performed on a personal computer with an Intel Core i7-7700HQ processor (2.80GHz CPU with 8GB RAM) using the ODE23 solver in MATLAB.

TABLE I
Controller and Filter Parameters

dc- and ac-side Filters		dc-link & Power Controllers		PLL	
$L_{\rm i}$	$23.1\,\mu{\rm H}$	$k_{\rm VC}^p$	$0.0865\,{\rm A/V^2}$	$k_{\rm PLL}^p$	$0.735\,{\rm rad/V}$
$R_{\rm i}$	$0.016\,\Omega$	$k_{\rm VC}^i$	$0.865\,{\rm A/(V^2 s)}$	$k_{\rm PLL}^i$	$5.88\,{\rm rad/(V\cdot s)}$
$C_{\rm f}$	$0.216\,{\rm mF}$	$k_{\rm Q}^i$	$0.0059\,{\rm V^{-1}}$	$\omega_{\rm c,PLL}$	$7854\,{\rm rad/s}$
$R_{\rm f}$	$0.462\,{\rm m\Omega}$	$k_{\rm Q}^i$	$0.059\,{\rm (V\cdot s)^{-1}}$		
$L_{\rm g}$	$23.1\,\mu{\rm H}$	$\omega_{\rm c,Q}$	$50.26\,{\rm rad/s}$	MPPT	
$R_{\rm g}$	$2.77\,{\rm m\Omega}$			$\omega_{\rm c,pv}$	$50.26\,{\rm rad/s}$
$C_{\rm dc}$	$0.1\,{\rm mF}$	Current Controller			
		$k_{\rm CC}^p$	$0.6\,{\rm V/A}$		
		$k_{\rm CC}^i$	$35\,{\rm V/(A\cdot s)}$		

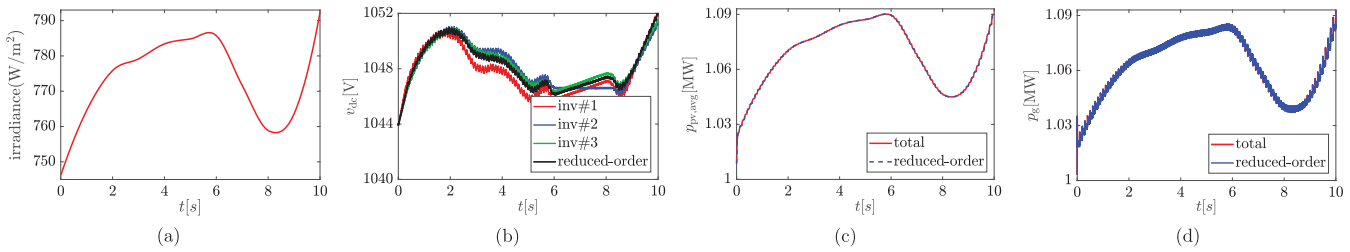

Fig. 3. (a) Incident solar irradiance. Simulation results for case #1 comparing the multi-inverter system and the corresponding reduced-order model of (b) dc-link voltage, (c) averaged PV power, and (d) injected real power to the grid.

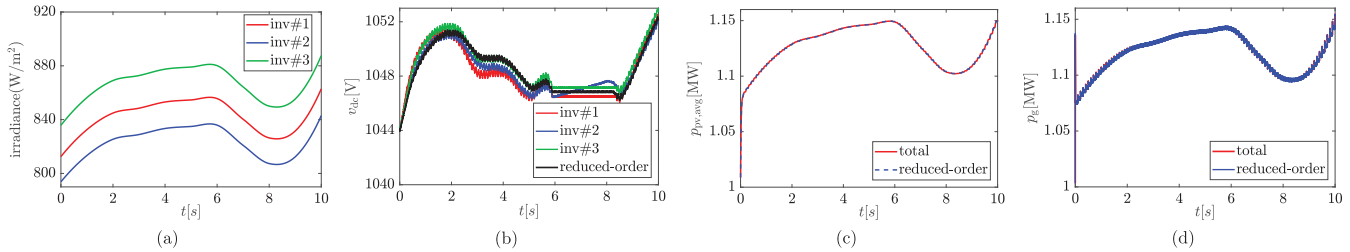

Fig. 4. (a) Incident solar irradiance for selected inverters. Simulation results for case #2 comparing the multi-inverter system and the corresponding reduced-order model of (b) dc-link voltage, (c) averaged PV power, and (d) injected real power to the grid.

The results for case #1 are shown in Figs. 3b–3d. Figure 3b shows the dc-link voltage of three inverters (selected arbitrarily) in the parallel system and that of the reduced-order model. Figure 3c compares the total averaged PV output power ($p_{\mathrm{pv,avg}}$) of the inverters in the system and the reduced-order model, and Fig. 3d plots the total injected real power to the grid of the multi-inverter system and the reduced-order model. Results indicate that despite variations in the operation of the MPPT algorithm in the inverters, the reduced-order model captures the total power of the parallel system closely. The results for case #2 are shown in Figs. 4b–4d. These figures establish the accuracy of the reduced-order model in spite of differences in the MPPT algorithm *and* solar irradiance. The computation times to simulate dynamics of all the inverters and that required for the reduced-order model for case #1 are 966.8 s and 91.2 s, respectively, and those for case #2 are 1128.9 s and 133.0 s, respectively. This clearly demonstrates the computational benefit of the aggregate model.

V. Concluding Remarks

In this paper we proposed a reduced-order aggregated model for parallel-connected three-phase PV inverters. We derived parametric scalings that allow one to represent a collection of N such inverters as a single aggregated inverter with the same structure and model order as that of an individual inverter. Future work will focus on developing analytical results for heterogeneous settings and applying these models to explore the performance of PV inverter systems alongside bulk-grid dynamics, particularly in low-inertia settings.

Acknowledgement

This work was supported in part by the U.S. Department of Energy (DOE) Solar Energy Technologies Office under Contract No. DE-EE0000-1583 and the National Science Foundation under award ECCS-1453921.

Appendix

Partition the state vector as $x = [x_{\mathrm{LCL}}^{\mathrm{T}}, x_{\mathrm{dc}}^{\mathrm{T}}, x_{\mathrm{RC}}^{\mathrm{T}}, x_{\mathrm{CC}}^{\mathrm{T}}, x_{\mathrm{PLL}}^{\mathrm{T}}]^{\mathrm{T}}$, where $x_{\mathrm{LCL}} := [i_{\mathrm{i}}^{\mathrm{d}}, i_{\mathrm{i}}^{\mathrm{q}}, i_{\mathrm{o}}^{\mathrm{d}}, i_{\mathrm{o}}^{\mathrm{q}}, v_{\mathrm{f}}^{\mathrm{d}}, v_{\mathrm{f}}^{\mathrm{q}}]^{\mathrm{T}}$, $x_{\mathrm{dc}} := [e_{\mathrm{dc}}, p_{\mathrm{pv,avg}}, \phi_{\mathrm{dc}}]^{\mathrm{T}}$, $x_{\mathrm{RC}} := [q_{\mathrm{avg}}, \phi_{\mathrm{q}}]^{\mathrm{T}}$, $x_{\mathrm{CC}} := [\gamma^{\mathrm{d}}, \gamma^{\mathrm{q}}]^{\mathrm{T}}$, and $x_{\mathrm{PLL}} := [v_{\mathrm{PLL}}, \phi_{\mathrm{PLL}}, \delta]^{\mathrm{T}}$. The inverter dynamics are

$$\begin{bmatrix} \dot{x}_{\mathrm{LCL}} \\ \dot{x}_{\mathrm{dc}} \\ \dot{x}_{\mathrm{RC}} \\ \dot{x}_{\mathrm{CC}} \\ \dot{x}_{\mathrm{PLL}} \end{bmatrix} = \begin{bmatrix} A_{\mathrm{LCL}} & A_{\mathrm{LCL}}^{\mathrm{dc}} & A_{\mathrm{LCL}}^{\mathrm{RC}} & A_{\mathrm{LCL}}^{\mathrm{CC}} & 0 \\ 0 & A_{\mathrm{dc}} & 0 & 0 & 0 \\ 0 & 0 & A_{\mathrm{RC}} & 0 & 0 \\ A_{\mathrm{CC}}^{\mathrm{LCL}} & A_{\mathrm{CC}}^{\mathrm{dc}} & A_{\mathrm{CC}}^{\mathrm{RC}} & 0 & 0 \\ 0 & 0 & 0 & 0 & A_{\mathrm{PLL}} \end{bmatrix} \begin{bmatrix} x_{\mathrm{LCL}} \\ x_{\mathrm{dc}} \\ x_{\mathrm{RC}} \\ x_{\mathrm{CC}} \\ x_{\mathrm{PLL}} \end{bmatrix} + g(x, u_1, u_2, u_3),$$

where the nonzero submatrices are given by

$$A_{\mathrm{LCL}} = \begin{bmatrix} -\frac{R_{\mathrm{i}}+k_{\mathrm{CC}}^p}{L_{\mathrm{i}}} & 0 & 0 \\ 0 & -\frac{R_{\mathrm{i}}+k_{\mathrm{CC}}^p}{L_{\mathrm{i}}} & 0 \\ 0 & 0 & -\frac{R_{\mathrm{g}}}{L_{\mathrm{g}}} \\ 0 & 0 & -2\pi \times 60 \\ -\frac{R_{\mathrm{f}}(k_{\mathrm{CC}}^p+R_{\mathrm{i}})}{L_{\mathrm{i}}} + \frac{1}{C_{\mathrm{f}}} & -(2\pi \times 60)R_{\mathrm{f}} & \frac{R_{\mathrm{f}}R_{\mathrm{g}}}{L_{\mathrm{g}}} - \frac{1}{C_{\mathrm{f}}} \\ (2\pi \times 60)R_{\mathrm{f}} & -\frac{R_{\mathrm{f}}(k_{\mathrm{CC}}^p+R_{\mathrm{i}})}{L_{\mathrm{i}}} & 0 \end{bmatrix}$$

$$\begin{bmatrix} 0 & -\frac{1}{L_{\mathrm{i}}} & 0 \\ 0 & 0 & -\frac{1}{L_{\mathrm{i}}} \\ 2\pi \times 60 & \frac{1}{L_{\mathrm{g}}} & 0 \\ -\frac{R_{\mathrm{g}}}{L_{\mathrm{g}}} & 0 & \frac{1}{L_{\mathrm{g}}} \\ 0 & -\frac{R_{\mathrm{f}}}{L_{\mathrm{i}}} - \frac{R_{\mathrm{f}}}{L_{\mathrm{g}}} & 2\pi \times 60 \\ \frac{R_{\mathrm{f}}R_{\mathrm{g}}}{L_{\mathrm{g}}} - \frac{1}{C_{\mathrm{f}}} & -2\pi \times 60 & -\frac{R_{\mathrm{f}}}{L_{\mathrm{i}}} - \frac{R_{\mathrm{f}}}{L_{\mathrm{g}}} \end{bmatrix},$$

$$A_{\mathrm{LCL}}^{\mathrm{dc}} = \begin{bmatrix} 0 & 0 \\ \frac{k_{\mathrm{CC}}^p k_{\mathrm{VC}}^p}{L_{\mathrm{i}}} & 0 & -\frac{k_{\mathrm{CC}}^p k_{\mathrm{VC}}^i}{L_{\mathrm{i}}} \\ 0 & 0 & 0 \\ 0 & 0 & 0 \\ \frac{k_{\mathrm{CC}}^p k_{\mathrm{VC}}^p R_{\mathrm{f}}}{L_{\mathrm{i}}} & 0 & -\frac{k_{\mathrm{CC}}^p k_{\mathrm{VC}}^i R_{\mathrm{f}}}{L_{\mathrm{i}}} \end{bmatrix},$$

$$A_{\rm CC}^{\rm LCL}=\begin{bmatrix}-1&0&0&0&0&0\\0&-1&0&0&0&0\end{bmatrix},A_{\rm CC}^{\rm dc}=\begin{bmatrix}0&0&0\\k_{\rm VC}^p&0&-k_{\rm VC}^i\end{bmatrix},$$

$$A_{\rm LCL}^{\rm RC}=\begin{bmatrix}-\frac{k_{\rm CC}^pk_{\rm Q}^p}{L_{\rm i}}&\frac{k_{\rm CC}^pk_{\rm Q}^i}{L_{\rm i}}\\0&0\\0&0\\0&0\\-\frac{k_{\rm CC}^pk_{\rm Q}^pR_{\rm f}}{L_{\rm i}}&\frac{k_{\rm CC}^pk_{\rm Q}^iR_{\rm f}}{L_{\rm i}}\\0&0\end{bmatrix},A_{\rm LCL}^{\rm CC}=\begin{bmatrix}\frac{k_{\rm CC}^i}{L_{\rm i}}&0\\0&\frac{k_{\rm CC}^i}{L_{\rm i}}\\0&0\\0&0\\\frac{k_{\rm CC}^iR_{\rm f}}{L_{\rm i}}&0\\0&\frac{k_{\rm CC}^iR_{\rm f}}{L_{\rm i}}\end{bmatrix},$$

$$A_{\rm dc}=\begin{bmatrix}0&0&0\\0&-\omega_{\rm c,pv}&0\\-1&0&0\end{bmatrix},A_{\rm RC}=\begin{bmatrix}-\omega_{\rm c,Q}&0\\0&-1\end{bmatrix},$$

$$A_{\rm CC}^{\rm RC}=\begin{bmatrix}-k_{\rm Q}^p&k_{\rm Q}^i\\0&0\end{bmatrix},A_{\rm PLL}=\begin{bmatrix}-\omega_{c,\rm PLL}&0&0\\-1&0&0\\-k_{\rm PLL}^p&k_{\rm PLL}^i&0\end{bmatrix}.$$

Let g_ℓ denote the ℓ-th entry of the function $g(x,u_1,u_2,u_3)$. The nonzero entries of $g(x,u_1,u_2,u_3)$ are given by

$$g_2=-\frac{k_{\rm CC}^pk_{\rm VC}^p}{L_{\rm i}}v_{\rm dc}^{\star2},\ g_8=\omega_{\rm c,pv}\sqrt{e_{\rm dc}}i_{\rm pv},\ g_9=v_{\rm dc}^{\star2},$$

$$g_3=(-k_{\rm PLL}^pv_{\rm PLL}+k_{\rm PLL}^i\phi_{\rm PLL})i_{\rm o}^{\rm q}-\frac{1}{L_{\rm g}}v_{\rm g}^{\rm d},\ g_{13}=-k_{\rm VC}^pv_{\rm dc}^{\star2}$$

$$g_4=(k_{\rm PLL}^pv_{\rm PLL}-k_{\rm PLL}^i\phi_{\rm PLL})i_{\rm o}^{\rm d}-\frac{1}{L_{\rm g}}v_{\rm g}^{\rm q},$$

$$g_5=(-k_{\rm PLL}^pv_{\rm PLL}+k_{\rm PLL}^i\phi_{\rm PLL})(-R_{\rm f}i_{\rm i}^{\rm q}+v_{\rm f}^{\rm q})+\frac{R_{\rm f}}{L_{\rm g}}v_{\rm g}^{\rm d},$$

$$g_6=(k_{\rm PLL}^pv_{\rm PLL}-k_{\rm PLL}^i\phi_{\rm PLL})(-R_{\rm f}i_{\rm i}^{\rm d}+v_{\rm f}^{\rm d})+\frac{R_{\rm f}}{L_{\rm g}}v_{\rm g}^{\rm q}$$

$$-\frac{R_{\rm f}k_{\rm CC}^pk_{\rm VC}^p}{L_{\rm i}}v_{\rm dc}^{\star2},g_7=\frac{1}{C_{\rm dc}}(\sqrt{e_{\rm dc}}i_{\rm pv}-\frac{3}{2}(v_{\rm i}^{\rm d}i_{\rm i}^{\rm d}+v_{\rm i}^{\rm q}i_{\rm i}^{\rm q})),$$

$$g_{10}=\frac{3}{2}\omega_{\rm c,Q}(v_{\rm g}^{\rm q}i_{\rm o}^{\rm d}-v_{\rm g}^{\rm d}i_{\rm o}^{\rm q}),\ g_{14}=\omega_{\rm c,PLL}v_{\rm g}^{\rm d},\ g_{16}=2\pi\times60.$$

REFERENCES

[1] M. Bolinger and J. Seel, "Utility-scale solar: Empirical trends in project technology, cost, performance, and ppa pricing in the united states – 2018 edition," https://emp.lbl.gov/sites/default/files/lbnl_utility_scale_solar_2018_edition_report.pdf, accessed: 2019-01-09.

[2] "String inverters power one of UK's largest solar parks," https://new.abb.com/power-converters-inverters/solar/utility-scale/string-inverters-power-one-of-uk-s-largest-solar-parks, accessed: 2019-01-15.

[3] Y. Jung, G. Yu, J. Choi, and J. Choi, "High-frequency dc link inverter for grid-connected photovoltaic system," in *Twenty-Ninth IEEE Photovoltaic Specialists Conference*, May 2002, pp. 1410–1413.

[4] A. Yazdani, A. R. Di Fazio, H. Ghoddami, M. Russo, M. Kazerani, J. Jatskevich, K. Strunz, S. Leva, and J. A. Martinez, "Modeling guidelines and a benchmark for power system simulation studies of three-phase single-stage photovoltaic systems," *IEEE Trans. Power Del.*, vol. 26, no. 2, pp. 1247–1264, Apr. 2011.

[5] T. Kerekes, R. Teodorescu, M. Liserre, C. Klumpner, and M. Sumner, "Evaluation of three-phase transformerless photovoltaic inverter topologies," *IEEE Trans. Power Electron.*, vol. 24, no. 9, pp. 2202–2211, Sep. 2009.

[6] H. N. Villegas Pico and B. B. Johnson, "Transient stability assessment of multi-machine multi-converter power systems," *IEEE Trans. Power Syst.*, 2019, to appear.

[7] L. Luo and S. V. Dhople, "Spatiotemporal model reduction of inverter-based islanded microgrids," *IEEE Trans. Energy Convers.*, vol. 29, no. 4, pp. 823–832, Dec. 2014.

[8] M. Rasheduzzaman, J. A. Mueller, and J. W. Kimball, "Reduced-order small-signal model of microgrid systems," *IEEE Trans. Sustain. Energy*, vol. 6, no. 4, pp. 1292–1305, Oct. 2015.

[9] O. O. Ajala, A. D. Domínguez-García, and P. W. Sauer, "A hierarchy of models for inverter-based microgrids," in *Energy Markets and Responsive Grids: Modeling, Control and Optimization*. Berlin: Springer-Verlag, 2017.

[10] V. Purba, S. V. Dhople, S. Jafarpour, F. Bullo, and B. B. Johnson, "Reduced-order structure-preserving model for parallel-connected three-phase grid-tied inverters," in *2017 IEEE 18th Workshop on Control and Modeling for Power Electronics*, Jul. 2017, pp. 1–7.

[11] V. Purba, B. B. Johnson, M. Rodriguez, S. Jafarpour, F. Bullo, and S. V. Dhople, "Reduced-order aggregate model for parallel-connected single-phase inverters," *IEEE Trans. Energy Convers.*, vol. 34, no. 2, pp. 824–837, Jun. 2019.

[12] A. Ghosh, "Dynamic modelling of an aggregated solar-PV system for power system transient stability studies," Master's thesis, University of Nottingham, 2018.

[13] S. Vijayshankar, V. Purba, P. J. Seiler, and S. V. Dhople, "Reduced-order aggregate dynamical model for wind farms," 2019, accepted to the 2019 IEEE Power and Energy Society General Meeting.

[14] V. Purba, S. V. Dhople, S. Jafarpour, F. Bullo, and B. B. Johnson, "Network-cognizant model reduction of grid-tied three-phase inverters," in *Allerton Conference on Communication, Control, and Computing*, Oct 2017, pp. 157–164.

[15] Z. Shuai, Y. Peng, X. Liu, Z. Li, J. M. Guerrero, and Z. J. Shen, "Dynamic equivalent modeling for multi-microgrid based on structure preservation method," *IEEE Trans. Smart Grid*, 2018, to appear.

[16] X. Zha, S. Liao, M. Huang, Z. Yang, and J. Sun, "Dynamic aggregation modeling of grid-connected inverters using Hamilton's-action-based coherent equivalence," *IEEE Trans. Ind. Electron.*, vol. 66, no. 8, pp. 6437–6448, Aug. 2019.

[17] E. C. Aprilia, "Modeling of photovoltaic (PV) inverter for power quality studies," Master's thesis, Eindhoven University of Technology, 2012.

[18] S. Eftekharnejad, V. Vittal, G. T. Heydt, B. Keel, and J. Loehr, "Impact of increased penetration of photovoltaic generation on power systems," *IEEE Trans. Power Syst.*, vol. 28, no. 2, pp. 893–901, May 2013.

[19] "Reliability Guideline Power Plant Model Verification for Inverter-Based Resources," https://www.nerc.com/comm/OC_Reliability_Guidelines_DL/PPMV_for_Inverter-Based_Resources.pdf, accessed: 2019-05-24.

[20] A. Ghosh, R. Patel, M. Datta, and L. Meegahapola, "Investigation of transient stability of a power network with solar-PV generation: Impact of loading level control strategy," in *2017 IEEE Innovative Smart Grid Technologies - Asia (ISGT-Asia)*, Dec 2017, pp. 1–6.

[21] S. S. Guggilam, C. Zhao, E. DallAnese, Y. C. Chen, and S. V. Dhople, "Optimizing DER participation in inertial and primary-frequency response," *IEEE Trans. Power Syst.*, vol. 33, no. 5, pp. 5194–5205, Sep. 2018.

[22] M. M. S. Khan, Y. Lin, B. Johnson, V. Purba, M. Sinha, and S. Dhople, "A reduced-order aggregated model for parallel inverter systems with virtual oscillator control," in *2018 IEEE 19th Workshop on Control and Modeling for Power Electronics (COMPEL)*, Jun. 2018, pp. 1–6.

[23] M. G. Villalva, J. R. Gazoli, and E. R. Filho, "Comprehensive approach to modeling and simulation of photovoltaic arrays," *IEEE Trans. Power Electron.*, vol. 24, no. 5, pp. 1198–1208, May 2009.

[24] A. A. A. Radwan and Y. A. I. Mohamed, "Power synchronization control for grid-connected current-source inverter-based photovoltaic systems," *IEEE Trans. Energy Convers.*, vol. 31, no. 3, pp. 1023–1036, Sep. 2016.

[25] A. Yazdani and R. Iravani, *Voltage-Sourced Converters in Power Systems*. Hoboken, NJ: John Wiley & Sons, Inc., 2010.

[26] B. B. Johnson, S. V. Dhople, J. L. Cale, A. O. Hamadeh, and P. T. Krein, "Oscillator-based inverter control for islanded three-phase microgrids," *IEEE Journ. Photovoltaics*, vol. 4, no. 1, pp. 387–395, Jan. 2014.

[27] "Conext CL125 string inverter," https://solar.schneider-electric.com/product/conext-cl125-string-inverter/, accessed: 2019-01-04.

[28] "First solar series 6$^{\rm TM}$," http://www.firstsolar.com/-/media/First-Solar/Technical-Documents/Series-6-Datasheets/Series-6-Datasheet.ashx, accessed: 2019-01-04.

[29] "Oahu solar measurement grid (1-year archive): 1-second solar irradiance; oahu, hawaii (data); NREL report no. DA-5500-56506," http://dx.doi.org/10.5439/1052451, accessed: 2019-01-04.